Chemosphere 280 (2021) 130636

Contents lists available at ScienceDirect

Chemosphere

journal homepage: www.elsevier.com/locate/chemosphere

# Investigation of the efficiency of BiOI/BiOCl composite photocatalysts using UV, cool and warm white LED light sources - Photon efficiency, toxicity, reusability, matrix effect, and energy consumption

Máté Náfrádi [a], Klara Hernadi [b, c], Zoltán Kónya [b], Tünde Alapi [a, *]

[a] Department of Inorganic and Analytical Chemistry, University of Szeged, H-6720, Szeged, Dóm tér 7, Hungary
[b] Department of Applied and Environmental Chemistry, University of Szeged, H-6720, Szeged, Rerrich Béla tér 1, Hungary
[c] Institute of Physical Metallurgy, Metal Forming and Nanotechnology, University of Miskolc, HU-3515, Miskolc, Egyetemváros, Hungary

## HIGHLIGHTS

- BiOI:BiOCl composites were synthesized and tested for photocatalytic applications.
- The efficiency of three different LED light sources was compared for excitation.
- Adsorption capacity and transformation efficiency for MO are highly correlated.
- 400–700 nm and 398 nm light are similarly efficient for BiOI:BiOCl excitation.
- Wastewater matrices and their components affect the adsorption and efficiency.

## GRAPHICAL ABSTRACT

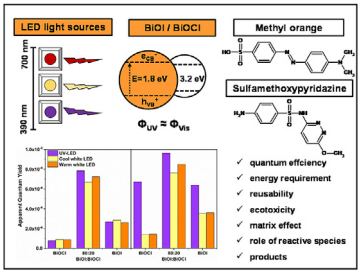


## ARTICLE INFO

*Article history:*
Received 31 January 2021
Received in revised form
10 April 2021
Accepted 19 April 2021
Available online 23 April 2021

Handling Editor: Yongmei Li

*Keywords:*
BiOX
Photocatalysis
Visible light
Quantum yield

## ABSTRACT

BiOI, BiOCl, and their composites (BiOI:BiOCl) with molar ratios from 95:5 to 5:95 were synthesized and tested in the transformation of methyl orange (MO) and sulfamethoxypyridazine (SMP) antibiotic, using three various LED light sources: UV LEDs (398 nm), cool and warm white LEDs (400–700 nm). The 80:20 BiOI:BiOCl photocatalyst showed the best adsorption capacity for MO and enhanced activity compared to BiOI and BiOCl. The apparent quantum yield ($\Phi_{app}$) of the MO and SMP transformation for cool and warm white light was slightly lower than for 398 nm UV radiation. The effect of methanol and 1,4-benzoquinone proved that the transformation is initiated mainly via direct charge transfer, resulting in the demethylation of MO and $SO_2$ extrusion from SMP. The change of photocatalytic efficiency was followed during three cycles. After the first one, the transformation rates decreased, but there was no significant difference between the second and third cycles. The decreased efficiency is most probably caused by the intermediates, whose continuous accumulation was observed during the cycles. Ecotoxicity measurements confirmed that no toxic substances were leached from the catalyst, but the transformation of both MO and SMP results in toxic intermediates. Using 80:20 BiOI:BiOCl and LED light source, the energy requirement of the removal is about half of the value determined using $TiO_2$ and a

* Corresponding author.
*E-mail address:* alapi@chem.u-szeged.hu (T. Alapi).

https://doi.org/10.1016/j.chemosphere.2021.130636

mercury vapor lamp. The effect of some components of wastewater ($Cl^-$, $HCO_3^-$ and humic acids), pH, and two matrices on the composite photocatalysts' efficiency and stability were also investigated.


## 1. Introduction

One of the current water treatment challenges is developing cost-effective post-treatment methods to remove hazardous, non-biodegradable contaminants having biological activity. Advanced Oxidation Processes (AOPs), as additive water treatment methods, offer a solution to this problem (Khan et al., 2019; Stefan, 2017). One of the widely investigated processes is heterogeneous photocatalysis, which is based on semiconductors' application. The widely used photocatalysts, $TiO_2$ and ZnO having wide band gaps; therefore, they are mainly active in the UV region (Konstantinou and Albanis, 2003), and the transformation of the organic substances is generally initiated by hydroxyl radical. Due to the absorption of a photon having appropriate energy, an electron ($e_{cb}^-$) in the excited conduction band and a hole ($h_{vb}^+$) in the valence band form and initiates the transformation of organic substances (Qian et al., 2019). The transformation can take place via direct charge transfer (Ahmed and Haider, 2018), photosensitization (Akpan and Hameed, 2009), or reaction with reactive oxygen species (ROS) (Konstantinou and Albanis, 2003). Their relative contribution to the transformation of target pollutants depends on the photocatalyst's chemical and surface properties, the substrate's properties, and the reaction parameters.

One of the main goals from a material science perspective is the synthesis of catalysts, which efficiently work under visible light radiation, as sunlight is our cheapest and inexhaustible energy source. Bismuth oxyhalides (BiOX: X = F, Cl, Br, I), as photoactive materials, have received widespread attention during the last decade. BiOF and BiOCl are active in the UV range (band gap: 3.6 eV for BiOF and 3.2 eV for BiOCl), while BiOBr, and especially BiOI are active in the visible range (band gap: 2.6 eV for BiOBr and 1.8 eV for BiOI) (Singh et al., 2018; Bárdos et al., 2019). Their advantages include excellent adsorption capacity, they are easy to synthesize, but the fast recombination of photoinduced charges decreases their efficiency (Cheng et al., 2014; Yao et al., 2020). Several attempts have been made to enhance the efficiency of BiOX photocatalysts, including the preparation of the composite catalysts. Composite materials, such as BiOCl/BiOBr (Jia et al., 2015; Zhang et al., 2020), BiOCl/BiOI, (Dong et al., 2012; Jiang et al., 2015; Shan et al., 2018; Siao et al., 2018; Wu et al., 2020; Xiao et al., 2012; Yang et al., 2016; Zhang et al., 2020; Zhong et al., 2018), $SiO_2$/BiOX (Shen et al., 2015) and $TiO_2$/BiOX (Dai et al., 2011; Liu et al., 2019), with improved stability and enhanced visible-light activity, were successfully synthesized. The activity improvement of the composite catalysts is explained by the synergetic effects of ion doping and heterostructure (Wang et al., 2020), the reduced recombination of electron-hole pairs (Shan et al., 2018), and highly enhanced adsorption capacity (Yang et al., 2016; Zhang et al., 2016, 2020). Methods such as the size-controlled synthesis of BiOX photocatalysts and the use of environmentally friendly, green synthesis methods were also investigated (Bárdos et al., 2019; Garg et al., 2018a, 2018b). Several studies are available about the structure, properties, and activity of BiOX photocatalysts. However, the effects of various reaction parameters that determine practical applicability, such as inorganic and organic wastewater components, and pH, have been rarely studied.

Due to the intensive development of optoelectronics in recent years, the use of light-emitting diodes (LEDs) radiating in the UV and visible light range has become increasingly popular. It makes possible to improve the efficiency of additive water treatment methods based on photochemical processes (Chen et al., 2017; Sergejevs et al., 2017). Compared to the conventional UV and visible light sources, LEDs have higher electric efficiency, lower price, better mechanical tolerance, and longer lifetime; therefore, they are a promising option for application in water treatment processes, which requires either visible or UV radiation (Jo and Tayade, 2014).

The present study aims to prepare composite BiOCl/BiOI photocatalysts with different molar ratios, to determine their absorption properties and photocatalytic activity, and to compare the apparent quantum yields using different LED light sources (398 nm UV, cool and warm white light). For evaluation of the photocatalytic performance of the pure BiOI, BiOCl, and the composites, the methyl orange (MO) dye and sulfamethoxypyridazine (SMP) antibiotic degradation was chosen. Toxicity measurements have also been performed to investigate the potential risk of using these photocatalysts. Also, studies of the effects of $Cl^-$, $HCO_3^-$, humic acid, pH and two matrices (river water and biologically treated domestic wastewater) provide information on the practical applicability of the best composite photocatalyst.

## 2. Materials and analytical methods

### 2.1. Materials

For the synthesis of photocatalysts, bismuth nitrate pentahydrate ($Bi(NO_3)_3 \times 5\ H_2O$, Alfa Aesar, 98%), potassium iodide and chloride (KI and KCl, Molar Chemicals, 99.7%), ethylene glycol (Sigma-Aldrich, 99.95%) and ethanol (VWR, 96%) were used without further purification. When the effect of additives was studied, NaCl (VWR, 99%), sodium-humate (Sigma Aldrich, tech. grade), methanol (VWR, 99.9%), and 1,4-benzoquinone (Acros Organics, 99%) were used. The pH of the solutions was adjusted with $H_2SO_4$ (Fluka, 49–51%) or NaOH (VWR, 98%) and measured with InoLab p730 pH meter. Methyl orange (MO) from VWR, (99%), sulfamethoxypyridazine (SMP) from Sigma Aldrich (99%) were purchased. NaF was from Alfa Aesar (99%). $O_2$ or $N_2$ gas (Messer Hungarogáz, 99.5% and 99.995%) was used to keep constant dissolved $O_2$ concentration. For the actinometric measurements $Fe_2(SO4)_3$ (VWR, 98%), potassium oxalate (Reanal, 98%), ammonium-reineckate (Sigma Aldrich, 93%), 1,10-phenanthroline (Sigma Aldrich, 99%), KOH (Fluka, 98%) and KSCN (VWR, 98%) was used.

Table S1 shows the date of matrices: river water (from Tisza, Szeged, Hungary) and the biologically treated domestic wastewater (from the water treatment plant, Szeged).

### 2.2. Preparation of BiOI/BiOCl composite catalysts

The BiOI and BiOCl photocatalysts were prepared as described in the literature (Bárdos et al., 2019). $Bi(NO_3)_3 \times 5\ H_2O$, KCl, and KI were used for preparation via a solvothermal method. The $Bi(NO_3)_3 \times 5\ H_2O$ and KCl, or KI was dissolved in 50 $cm^3$ ethylene glycol with continuous stirring and heating (up to 45 °C). The

suspension was heat-treated for 3 h at 120 °C in a PTFE-coated steel autoclave. The solid material was washed with distilled water and ethanol, then vacuum-filtered with a 0.1 μm pore size filter (Durapore®, hydrophilic PVDF) and dried for 24 h at 40 °C. The composite catalysts were prepared with the same method, with the addition of KCl and KI at the appropriate molar ratios. The molar ratios have been calculated to result in composites with 5.0–95.0 n/n% BiOI content. The color of the prepared materials changed from white to red, with increasing BiOI content (Fig. 2/a).

### 2.3. Photocatalytic test reactions

In each case, 100 $cm^3$ suspension was irradiated in a cylindrical glass reactor (inner diameter: 45 mm). For determination of the amount of adsorbed MO and SMP, the suspensions were stirred in the dark for 30 min before photocatalytic tests. The experiments were started by turning on the light source. $O_2$ or $N_2$ gas was continuously bubbled through the suspension to keep a constant dissolved $O_2$ concentration.

Fig. S2 shows the emission spectra of the LED light sources. Three different LED light sources were used; commercial 'UV' (LEDmaster, $\lambda_{emission} = 398 \pm 10$ nm, 288 lumens, 4.6 W), 'cool white' (LEDmaster, $\lambda_{emission} = 400–650$ nm, 390 lumens, 4.6 W), and 'warm white' (LEDmaster, $\lambda_{emission} = 400–700$ nm, 600 lumens, 4.6 W). 1.0 m of LED tape (60 LED/meter) was fixed on the inside of the aluminum, double-walled reactor having 66 mm inner diameter. The reactors were equipped with a water cooling system to ensure the LEDs' constant light output. The electrical power required to operate the LEDs was the same (4.6 W) in all cases; thus, the efficiency of the photocatalysts was determined at the same electrical energy input.

A widely used and commercially available photocatalyst, $TiO_2$ Aeroxide P25® (Acros Organics, 35–65 $m^2\ g^{-1}$ specific surface area) was used as a reference measurement. The irradiation of $TiO_2$ was performed using a fluorescent mercury vapor lamp (Lighttech; GCL303T5/UVA; 307 mm × 20.5 mm; 15 W) emitting in the 300–400 nm range ($\lambda_{max} = 365$ nm). The suspension was irradiated in a 500 $cm^3$ cylindrical glass reactor.

### 2.4. Analytical methods

The emission spectra of the LED light sources (Fig. S2) were recorded using a two-channel fiber-optic CCD spectrometer (AvaSpec-FT2048) in the 180–880 nm wavelength range. The photon flux of the light sources was determined using two chemical actinometry methods: Reinecke's salt (Wegner and Adamson, 1966) and the widely applied ferrioxalate (Hatchard and Parker, 1956) actinometry. Reinecke's salt actinometry can be involved mainly in the range of visible light; the quantum yield of the photolysis of Reinecke's salt changes from 0.311 to 0.270 in the 400–600 nm region (Kuhn et al., 2004). The 0.01 M solutions of potassium-reineckate were prepared (Cornet et al., 1997). The photon flux was calculated from the formation rate of $SCN^-$ determined via spectrophotometry with excess $Fe(NO_3)_3$. The molar absorption coefficient of FeSCN (3188 $mol^{-1}\ dm^3\ cm^{-1}$) was determined from the slope of its calibration curve.

The ferrioxalate actinometry can be used in the UV and near-UV region (254–500 nm). This method is based on the photoreduction of $K_3Fe(C_2O_4)_3$, and the quantification of the $Fe^{2+}$ ions is performed by complexation with 1,10-phenanthroline. Within the range of 365–514 nm, the quantum yield of the $Fe^{2+}$ formation changes from 1.2 to 0.93 (Kuhn et al., 2004).

The photocatalysts adsorb well the MO dye. NaF solution (0.5 $cm^3$, 0.5 M) was added to the samples (1.0 $cm^3$) for effective desorption of MO and its intermediates. After adding the NaF solution, the sample was kept for 10 min in the dark and finally centrifuged (Dragonlab, 15000 RPM), and filtered with syringe filters (0.22 μm, FilterBiO, PVDF-L). The recovery was checked with $2.0 \times 10^{-4}$ M concentration of MO in 0.50 g $dm^{-3}$ BiOCl and BiOI containing suspensions and was found to be 98(±1) % in both cases.

For spectrophotometric measurements, an Agilent 8453 UV–Vis spectrophotometer was used. The molar absorbance of MO (at 464 nm) and SMP (at 261 nm) is 25905 and 18990 $mol^{-1}\ dm^3\ cm^{-1}$, respectively. KI solution was used to determine the concentration of dissolved $I^-$. The absorbance was measured at 226 nm, the molar absorbance of $I^-$ at this wavelength was 13080 $mol^{-1}\ dm^3\ cm^{-1}$.

HPLC measurements were performed with an Agilent 1100 HPLC equipped with a diode array UV detector (DAD) to separate the intermediates and determine MO and SMP concentration in the treated suspension. For MO containing samples, the stationary phase was a Kinetex 2.6u XB-C18 100 A (Phenomenex) reverse phase column, while the mobile phase consisted of 40 v/v% acetonitrile (VWR, UPLC-grade) and 60 v/v% formic acid solution (0.1%). For SMP containing samples the same stationary phase was used, the mobile phase consisted of 12.5 v/v% acetonitrile and 87.5 v/v% formic acid. The flow rate of eluent was 0.70 ml $min^{-1}$, and the temperature was 25 °C. The products were determined via mass spectrometry (Agilent LC/MSD/VL with ESI source). Measurement was performed in positive mode (3500 V capillary voltage, 75 V fragmentor voltage), the scan range was 100–500 AMU.

Ecotoxicity test (LCK480, Hach-Lange) based on the bioluminescence measurements of *Vibrio fischeri* bacteria were used to determine the acute ecotoxicity of the samples. The inhibition of bioluminescence was measured using a Lumistox 300 (Hach Lange) luminometer after 30 min incubation time. For elimination of the formed $H_2O_2$, catalase enzyme (2000–5000 unit $mg^{-1}$, Sigma Aldrich) was added to the samples in 2.0 mg $dm^{-3}$ concentration.

The synthesized catalysts were characterized using powder X-ray diffractometry (XRD) (Rigaku Miniflex II, Cu Kα radiation source, 5.0–90.0 2Theta° range, with 4.0 2Theta° $min^{-1}$ resolution). The specific surface area was determined via $N_2$ adsorption/desorption isotherms using a Quantachrome NOVA 2200 analyser. The pore size distribution was calculated by the BJH method. Diffuse reflectance spectroscopy (DRS) was performed using an Ocean Optics DH-2000 light source and Ocean Optics USB4000 detector. The band gap energy values were evaluated by the Kubelka-Munk approach and the Tauc plot (Tauc, 1968) and reinforced by the first derivative approach method (Flak et al., 2013). X-ray photoelectron spectroscopy (Kratos XSAM-800 apparatus, non-monochromatic Mg Kα X-ray source) was adopted to investigate the surface elemental composition.

## 3. Results and discussion

### 3.1. Characterization of the photocatalysts

The XRD patterns of the synthesized pure BiOX (X = Cl, I) and their composites were compared (Fig. 1). The diffraction peaks can be indexed to the tetragonal BiOI and BiOCl phase (Bárdos et al., 2019). In the case of 50:50 M ratios, peaks of both components could be detected. The BiOI/BiOCl composites containing 20:80 and 80:20 BiOCl:BiOI molar ratios exhibit the characteristic peaks of pure BiOI or BiOCl (the main component). Comparing the profiles of BiOI with BiOI:BiOCl composite having 80:20 M ratio, it can be seen that the diffraction peaks slightly shift to the higher angles, corresponding to a smaller spacing distance between the different planes. The same phenomenon is less pronounced for BiOI:BiOCl composite having a 20:80 M ratio. Moreover, the diffraction peaks of composite are broader than the corresponding peaks of pure

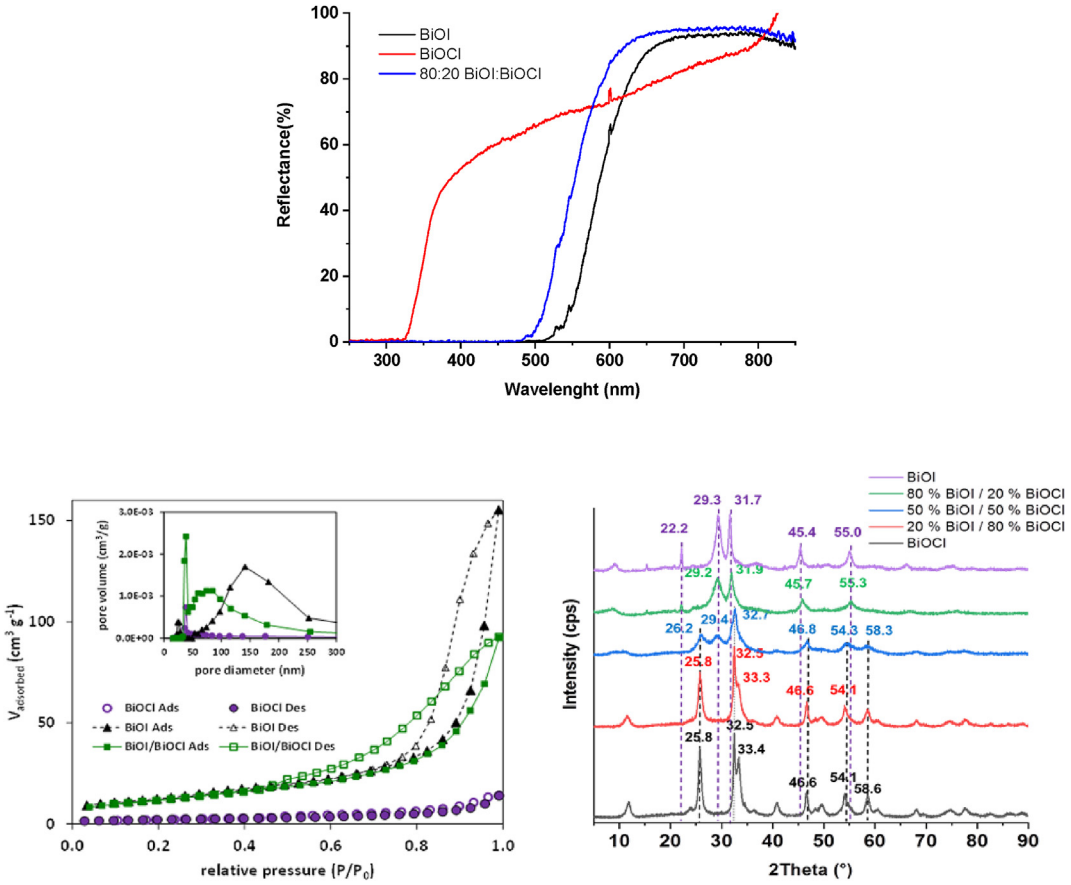


**Fig. 1.** UV–Vis DRS spectra, $N_2$ adsorption and desorption isotherms and the corresponding pore-size distribution (inset) and XRD patterns of BiOCl, BiOI, and their composites.

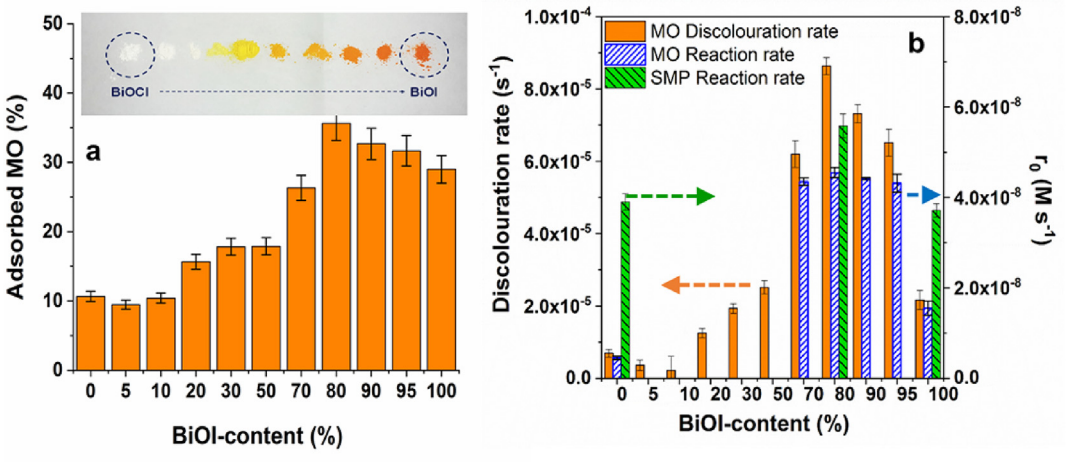


**Fig. 2.** The relative adsorbed amount of MO ($2.0 \times 10^{-4}$ M; 0.5 g $dm^{-3}$ photocatalyst) (a), the rate of discoloration (based on the absorbance determined at 464 nm), and the initial reaction rate ($r_0$) of MO and SMP determined by HPLC-DAD (b) using photocatalysts having various BiOI content.

BiOX, indicating the smaller crystallite sizes during heterogeneous growth (Ahern et al., 2015).

Specific surface area of the photocatalysts, total pore volume and average pore diameter are presented in Table 1. The hysteresis loop of the isotherm in the range of 0.6–1.0 $P/P_0$ (Fig. 1), suggests the formation of capillary condensation related to pores between closely-packed particles. The surface area of BiOI is much larger than the surface area of BiOCl and is similar to that of a composite catalyst with 80% BiOI content (Table 1.).

To analyze the surface chemical composition X-ray photoelectron spectroscopy (XPS) were conducted. The overall surface chemical compositions including atomic concentrations of the major elements are listed in Table 1. The atomic ratio of I:Cl on the surface of the composite catalyst is 9.7:2; higher than 8:2, which was applied for the catalyst preparation, and indicates a high concentration of $I^-$ on the surface. For BiOCl, the relative low atomic

**Table 1**
The specific surface areas, pore structures, band gap values and surface atomic composition of the photocatalysts.

| | | BiOI | BiOCl | 80:20 BiOI/BIOCl |
|---|---|---|---|---|
| **Surface Area ($m^2\ g^{-1}$)** | | 45.7 | 7.4 | 43.1 |
| **Pore Volume ($cm^3\ g^{-1}$)** | | 0.15 | 0.015 | 0.10 |
| **Average Pore Size (nm)** | | 141 | 38 | 39 |
| **Band gap (eV)** | | 2.20 | 3.41 | 2.41 |
| **Surface atomic composition (%)** | **O 1s** | 31.1 | 15.1 | 25.7 |
| | **Bi 4f** | 20.4 | 20.6 | 22.7 |
| | **I 3d** | 13.8 | – | 12.6 |
| | **Cl 2p** | – | 21.3 | 2.6 |

content of O 1s is due to the lack of surface hydroxyl group (Fig. S1) (Di et al., 2016; Hao et al., 2017; Liu and Wang, 2016).

Fig. 1 display the UV–Vis diffuse reflectance spectra of the BiOI, BiOCl and the 80:20 BiOI:BiOCl composite having best photocatalytic performance. While considering the optical properties of the investigated semiconductors the band gap energy for BiOCl was 3.41 eV, which is near to that reported in the literature (Ganose et al., 2016). Also, an interesting spectral feature was observed for this sample; its light absorption extends in the visible region. Although, this is unusual, it is not surprising as it can be related to the UV light induced formation of oxygen vacancies. This can be the reason of that, under UV radiation (even at 398 nm), the white color of BiOCl changes to grey, and then, after switching off the light, it returns to white in air. In the case of BiOI 2.20 eV was the band gap value, which is slightly different from what expected (~2.00 eV(Ganose et al., 2016)). This means that $Bi_5O_7I$ could be present in the sample, a material which is often a co-product of BiOI synthesis (Liu and Wang, 2016). For 80:20 BiOI/BiOCl composite, 2.41 eV, 0.2 eV higher band gap value was determined than that of BiOI sample, which points out the influence of BiOCl.

### 3.2. Characterization of the light sources

The light source usually determines the efficiency of each photochemical method. The emission spectra of the LED light sources are presented in Fig. S2. The UV LED's photon flux emitting at 398 ± 10 nm light was determined and compared by Reinecke'salt actinometry and ferrioxalate actinometry. Both methods can be applied for the determination of the photon flux of this light source. The values determined by Reinecke'salt actinometry was $5.81(\pm0.03) \times 10^{-6}$ $mol_{photon}$ $s^{-1}$, and a slightly lower value, $(5.12 \pm 0.02) \times 10^{-6}$ $mol_{photon}$ $s^{-1}$ was obtained by ferrioxalate actinometry (Hatchard and Parker, 1956).

The photon flux was $3.47(\pm0.25) \times 10^{-6}$ $mol_{photon}$ $s^{-1}$ for cool white LEDs, and $3.25(\pm0.25) \times 10^{-6}$ $mol_{photon}$ $s^{-1}$ for the warm white LEDs. Both values were obtained by Reinecke's salt actinometry and were about 40% of the UV LED's photon flux. Ferrioxalate actinometry provided much lower values since this method is suitable for determining the photon flux with a wavelength of shorter than 500 nm. In this way, the photon flux for cool white LEDs was $9.35(\pm0.65) \times 10^{-7}$ $mol_{photon}$ $s^{-1}$, about 20% of the UV-LED's photon flux. This value was slightly lower ($7.76(\pm0.73) \times 10^{-7}$ $mol_{photon}$ $s^{-1}$) for the warm white LEDs. For calculation of the apparent quantum yield of the transformation, the photon flux determined by Reinecke'salt actinometry was applied.

### 3.3. Adsorption properties

Adsorption generally plays a crucial role in heterogeneous photocatalysis, especially in the conversion of dyes. The relative adsorbed amount of MO ($2.0 \times 10^{-4}$ M) in a suspension containing 0.5 g $dm^{-3}$ catalyst was 29% and 11% for BiOI and BiOCl, respectively. This can be partly explained by the difference between the specific surface area (Table 1) and surface charge of BiOI and BiOCl. BiOI has a positive (Yusoff et al., 2019), while BiOCl particles possess negative surface charges over a wide pH range (Xiao et al., 2016; Zhao et al., 2018). MO is an azo dye with a pKa value of 3.46. The pH of the suspensions was 6.5, the MO was in deprotonated form having a negative charge. Due to the electrostatic interaction, adsorption of MO is most probably preferred on the surface of the BiOI. In the case of the composite catalysts, the amount of adsorbed MO increased with increasing the BiOI content, up to 80:20 M ratio, when 35.6(±2.5)% was adsorbed, and slightly decreased with the further increase of the BiOI content (Fig. 2/a). Adsorption of SMP was not measurable for either BiOI or BiOCl.

### 3.4. The photocatalytic test reactions using UV LEDs

The relative contribution of the direct UV photolysis (398 nm irradiation) to the transformation of MO and SMP was negligible. The effect of suspension concentration on the transformation rate was investigated using 80:20 BiOI:BiOCl composite photocatalyst. Within the range of 0.5–1.5 g $dm^{-3}$, amount of adsorbed MO and its transformation rate increased linearly (Fig. S3). Similar trend was observed for SMP. In further experiments, 0.5 g $dm^{-3}$ photocatalyst load was used to ensure adequate depth of light penetration into the suspension.

The interaction between the MO and the catalyst's surface requires the differentiation between the adsorbed and transformed amount of dye. Before determining MO concentration of the treated solution, NaF was added to the sample for desorption. In this way, the total amount of non-transformed MO can be measured. The initial transformation rate determined without NaF addition ($2.40 \times 10^{-8}$ M $s^{-1}$) is only 41% of the value determined after the addition of NaF ($4.10 \times 10^{-7}$ M $s^{-1}$) to the samples (Fig. S4). Above ~40% conversion, there is no significant effect of NaF addition, which can be explained by the competitive adsorption between MO and its products. The transformation is likely to result in products that successfully compete with MO for adsorption sites. The pH of the suspension does not change significantly (from 6.5 to 6.2) during the transformation.

For MO, significantly increased activity was determined for the composite catalysts having more than 50% BiOI content. The discoloration rate reached the maximum value in the range of 70–95% BiOI content (Fig. 2b). Adsorption capacity and transformation efficiency are correlated (Fig. 2).

In the spectrophotometric measurements, the characteristic change of the shape of the MO spectrum and the shift of its maximum to the lower wavelengths indicates the formation of products having significant absorption around 400–450 nm (Fig. S6). Therefore, the HPLC-DAD method was used to determine the initial transformation rate of MO for the most promising composite catalysts (70, 80, 90, and 95% BiOI content), the pure

BiOI, and BiOCl (Fig. 2b). For SMP, the HPLC-DAD method was used to determine the concentration in each case because of the formation of aromatic intermediates. The initial transformation rate of MO correlated with the discoloration rate: it was about three times higher for composite catalysts than for BiOI.

The photocatalytic activity of pure BiOCl, BiOI, and the 80:20 BiOI:BiOCl composite catalysts having the best adsorption properties were tested and compared using the UV LEDs (398 nm) light source. The initial transformation rate of MO was significantly higher for BiOI with a larger surface area and smaller bandgap value than for BiOCl. (Table 1). Surprisingly, the non-adsorbed SMP transformation takes place with similar rate in the case of both pristine photocatalysts. For BiOI, the transformation rate was doubled, while for BiOCl, a five time higher transformation rate was determined for SMP than for MO. The reason can be the UV light induced formation of oxygen vacancies in BiOCl and consequently extending the excitability to larger (above 363 nm) wavelength ranges. The composite catalyst showed increased activity to transform both components compared to the pure BiOI and BiOCl.

### 3.5. Comparison of the efficiency using UV, cool, and warm white LEDs

The activity of the catalysts were determined under visible light irradiation, using cool white and warm white light and compared to the activity determined under 398 nm UV irradiation (Fig. 3). For both organic substances, the transformation rate was significantly higher using 398 nm irradiation than visible light, similarly, the product formation was markedly faster (Fig. S5). Both BiOI and the composite catalyst proved better activity than BiOCl under visible light irradiation. There was no difference between the initial transformation rates determined in the case of cool white and warm white light. The excellent behaviour of the composite was also manifested under excitation with visible light. Opposite to the BiOI:BiOCl composite catalyst, an induction period can be observed (up to 30 min) when pure BiOI was used for MO degradation. During this period the transformation rate increased with the increased average energy of the photons (UV < Cool white < Warm white) (Fig. S5).

Since there is a significant difference between the photon flux of each light source and the energy of the emitted photons, it is worth comparing the efficiency based on the apparent quantum yields ($\Phi_{app}$ = number of photons reached the treated suspension/number of molecule transformed) of the transformation. The photon flux of visible light LEDs ($3.47(\pm0.25) \times 10^{-6}$ $mol_{photon}$ $s^{-1}$ for the cool and $3.25(\pm0.25) \times 10^{-6}$ $mol_{photon}$ $s^{-1}$ for the warm white LEDs) is about 40% of the photon flux of UV LEDs ($5.81(\pm0.03) \times 10^{-6}$ $mol_{photon}$ $s^{-1}$). Also, photons' average energy is lower, as these LEDs emit light primarily in the 400–700 nm range. The flux of photons with a wavelength shorter than 500 nm for cool ($9.35(\pm0.65) \times 10^{-7}$ $mol_{photon}$ $s^{-1}$)) and warm white LEDs ($7.76(\pm0.73) \times 10^{-7}$ $mol_{photon}$ $s^{-1}$) is less than 20% of the photon flux of UV-LEDs ($5.81 \pm 0.03) \times 10^{-6}$ $mol_{photon}$ $s^{-1}$).

In the case of MO using 398 nm light, the value of $\Phi_{app}$ was much higher for BiOI than for BiOCl, while for SMP there was no significant difference between them. In the case of MO transformation, the $\Phi_{app}$ measured for the composite was nearly double than the $\Phi_{app}$ of BiOI, regardless of the light source (Fig. 3), and the $\Phi_{app}$ for cool and warm white light was just slightly lower than, for 398 nm UV irradiation. This suggests that BiOI and BiOI:BiOCl composite can utilize visible and near-UV light with similar efficiency for the well-absorbed MO transformation. For SMP, both pristine catalysts showed better activity than for MO. The $\Phi_{app}$ for 398 nm was higher than for visible light excitation for pristine catalysts, even for BiOCl. Similarly to MO, a significantly increased $\Phi_{app}$ values were determined in the case of the composite catalyst and the difference between the values obtained for visible and UV light excitation practically disappeared.

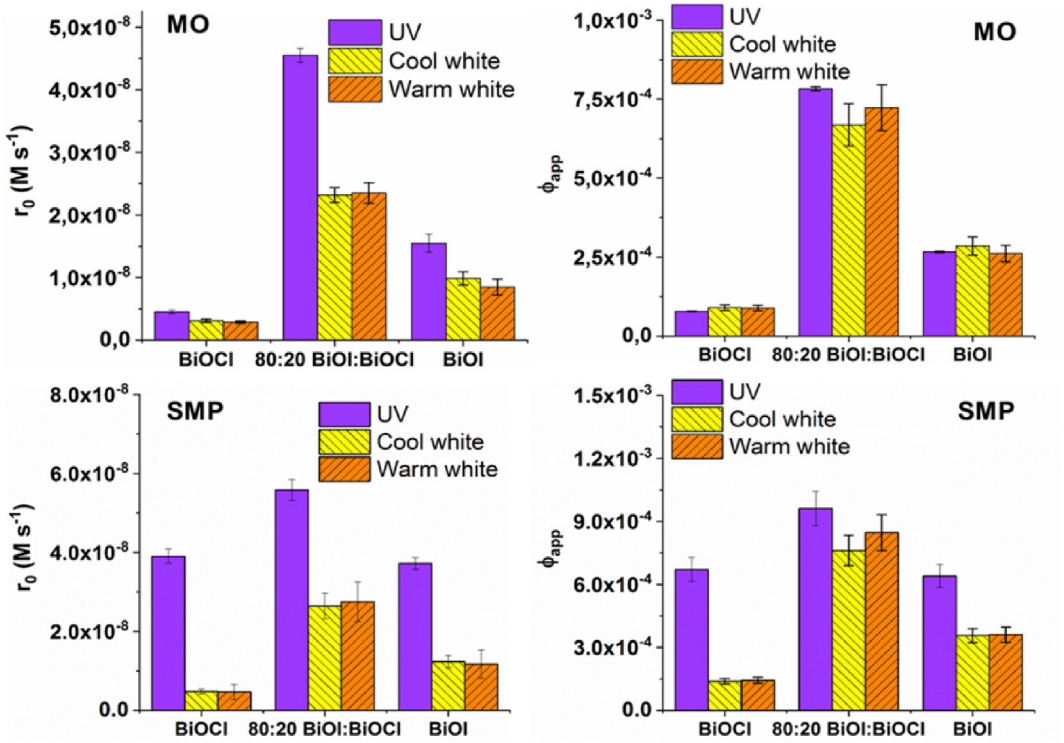


**Fig. 3.** The initial transformation rate ($r_0$) and apparent quantum yield ($\Phi_{app}$) of the MO and SMP transformation.

The transformation rate and the $\Phi_{app}$ value increases with the catalyst concentration (Fig. S3) because the higher surface area increases the number of photogenerated charges. The excellent adsorption properties of the photocatalyst can also contribute to this. Thus, using 1.5 g $dm^{-3}$ BiOI:BiOCl composite suspension, the $\Phi_{app}$ determined in 398 nm irradiated suspensions are about three times higher than in the case of 0.5 g $dm^{-3}$ suspensions.

### 3.6. The role of reactive species

For BiOX photocatalysts, the mechanism of transformation is not yet clear; the OH•-based reaction (Garg et al., 2018a), direct charge transfer (Dai et al., 2007; Garg et al., 2018a) and/or reaction with $O_2^{\bullet-}$ (Yang et al., 2020), as well as photosensitization (Li et al., 2011) were also reported.

Fónagy et al. (2021) evidently demonstrated that 1,4-BQ can be used as $e_{cb}^-$ scavenger in $O_2$-free suspension, and the amount of the formed 1,4-$H_2Q$ is proportional to the amount of the photogenerated $e_{cb}^-$. Thus, we studied the reduction of 1,4-BQ into 1,4-$H_2Q$ in $O_2$-free and the backward reaction in $O_2$-saturated suspensions under 398 nm radiation (Fig. 4). The transformation of 1,4-$H_2Q$ to 1,4-BQ relates to the reaction with $h_{vb}^+$, while the reaction between 1,4-$H_2Q$ and $O_2^{\bullet-}$ is responsible mainly for ring-opening processes and mineralization (Fónagy et al., 2021).

(interrupted lines show when $N_2$ bubbling was changed to $O_2$ bubbling).

The transformation of 1,4-BQ was faster using the composite compared to BiOI, due to the heterojunction between BiOI and BiOCl, which could prevent the charge carrier recombination more efficiently and improve the photocatalytic performance by this way. The 1,4-BQ completely transformed into 1,4-$H_2Q$ in $O_2$-free suspensions. Replacing $N_2$ to $O_2$, 80% (BiOI) and 70% (composite) of $H_2Q$ oxidized back into 1,4-BQ extremely quick, (Fig. 4). The behaviour of BiOCl was quite different: only a small fraction of $H_2Q$ could be transformed back to BQ in $O_2$-containing suspension, and its transformation takes place, which is most probably caused by the reaction with $O_2^{\bullet-}$ and results in ring-opening products. The transformation of $H_2Q$ in $O_2$ saturated suspension is negligible for BiOI, but happens for composite (Fig. 4). The UV light induced formation of oxygen vacancies in BiOCl can be the reason of the high activity of BiOCl under 398 nm irradiation, opposite that, the excitation of pure BiOCl (band gap: 3.41 eV, Table 1.) requires irradiation with wavelength shorter than 363 nm. The white color of BiOCl changes to grey under 398 nm irradiation, which was not observed under visible light irradiation.

In agreement with the published results of Fónagy et al. (2021) and Xie et al. (2018) we can conclude that, in $O_2$ containing suspension of BiOCl, the excitation with 398 nm results in $O_2^{\bullet-}$ formation, which can contribute to the transformation of organic substances. For pure BiOI, there is no $O_2^{\bullet-}$ formation, and the direct charge transfer is responsible for the transformation of organic substances. The improved photocatalytic performance of the composite is due to the combination of the heterojunction between BiOI and BiOCl, and the possibility of $O_2^{\bullet-}$ formation.

In $O_2$-containing suspensions, methanol ($1.0 \times 10^{-2}$ M) as OH• scavenger does not affect the transformation rate of MO and SMP, even in the case of BiOCl, proving that this reactive species has no role in the transformation. Addition of 1,4-BQ ($1.0 \times 10^{-2}$ M) reduced the transformation rate of MO by 84%, but no effect was observed in the case of SMP. In MO containing suspension the 1,4-BQ transformation was much slower than in SMP containing suspension. The lack of dissolved $O_2$ also decreased the conversion, but to a different extent: by 70% for well-adsorbed MO and by 34% for poorly adsorbed SMP (Fig. 5). The relatively rapid conversion of SMP in an $O_2$-free suspension suggests reaction with both photogenerated charges, so SMP partially could take over the role of $O_2$ as an $e_{cb}^-$ scavenger, which facilitates the reaction with the $h_{vb}^+$. This is supported by the high value of the rate constant between the sulfonamides and the $e_{aq}^-$ (Mezyk et al., 2007), but further studies are needed to clarify this hypothesis.

In the case of BiOI and BiOI:BiOCl photocatalyst, the main product of MO is formed by demethylation (Fig. S6), which confirms the important role of the direct charge transfer in MO conversion (Dai et al., 2007). For $TiO_2$ P25, the hydroxylation and demethylation occurs parallel (Dai et al., 2007), and both products

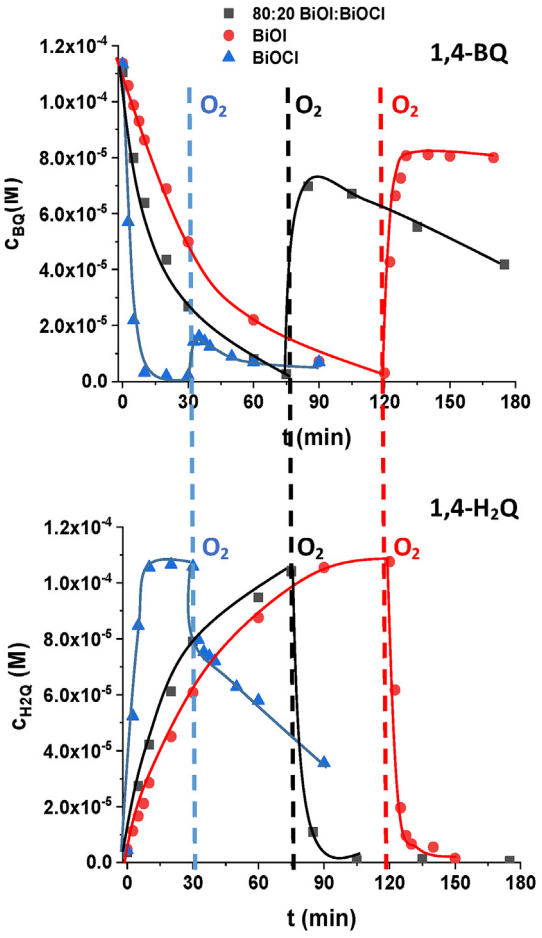


**Fig. 4.** The concentration of 1,4-BQ and 1,4-$H_2Q$ in $O_2$-free (before interrupted line) and in $O_2$ saturated (after interrupted line) suspensions under 398 nm irradiation.

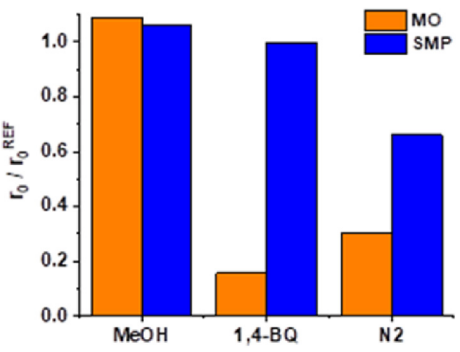


**Fig. 5.** Effect of methanol, 1,4-BQ in air saturated 80:20 BiOI:BiOCl suspensions and the relative transformation rates in $O_2$-free suspensions.

are formed at a similar rate (Fig. S6). The hydroxylated product results in a red-shift of the UV–Vis spectra, compared to the blue-shift associated with the product formed via demethylation. For SMP the main product is formed via $SO_2$ extrusion (Khaleel et al., 2013), as LC/MS measurements proved that. The formation of hydroxylated products was not observed for any of the target compounds when BiOI, BiOCl or composite catalysts were used opposite to the application of P25 (Fig. S6). This observation is in agreement with the negligible effect of methanol.

### 3.7. Reusability of the composite catalyst

The study of the stability and reusability of the catalyst has a crucial role in practical application. Degradation of MO and SMP was monitored for three consecutive cycles (Fig. 6), using the 80:20 BiOI:BiOCl composite catalyst. After complete transformation (end of the cycle), the initial concentration was adjusted to $1.0 \times 10^{-4}$ M by adding a small volume of concentrated solution. The transformation rate of both target substances decreased after the first cycle, but there was no difference between the values determined for the second and third cycles. Decreased activity may be due to the accumulation of products and their competition with MO and SMP for surface active sites and reactive species. There is no significant change in the XRD patterns after the third cycle; thus, there is probably no change in the photocatalyst structure.

### 3.8. Effect of pH, matrix components and matrices

The effect of parameters important for practical applicability, thus pH, $Cl^-$ (120 mg $dm^{-3}$), $HCO_3^-$ (525 mg $dm^{-3}$), Na-humate (20 mg $dm^{-3}$) and two matrices (biologically treated domestic wastewater and river water) on the efficiency was investigated. The concentration of additives was adjusted to the average concentration of biologically treated wastewater. Table S1 shows the chemical parameters of the matrices.

The pH of the solution was adjusted to 9.2 and 4.0 with NaOH and $H_2SO_4$ solutions, respectively. The addition of BiOI:BiOCl catalyst restored the pH of the suspension to around 6.5. The protonation-deprotonation process of MO (pKa = 3.46) could not affect its adsorption. Nevertheless, the relative amount of adsorbed MO (from 36% to 21% and 27%) and the conversion rate (to 45% and 53%) was significantly reduced (Fig. 7). The ionic components can change the surface properties and electrostatic attraction between photocatalyst and substrate, thereby affect the photodegradation. NaCl decreased the adsorption of MO (to 16%) and its conversion rate (to 49%), but increased the transformation rate of SMP (by 46%). A significant change was observed when 525 mg $dm^{-3}$ $NaHCO_3$ was added to the suspension. The transformation rate of MO was completely and of SMP partly (to 58%) inhibited. MO practically did not adsorb in this case. Spectrophotometric measurements show that the concentration of $I^-$ in the solution did not change due to the addition of NaOH, but $H_2SO_4$ and NaCl, and even $NaHCO_3$ increased that, suggesting a change in the surface of the catalyst (Fig. 7). The relative high $I^-$ concentration in the suspension proved that $HCO_3^-$ dramatically changed the photocatalyst. To accurately explain these results, further studies are needed on the effect of different ions on the surface properties and on the stability of the BiOI:BiOCl photocatalyst.

The humic acids and humates often compete for adsorption sites with the pollutants. As our results show, humate decreased the transformation of MO and SMP to a similar extent. $I^-$ leaching was not observed, but the relative adsorbed amount of MO decreased to 21% (Fig. 7). Using river water and biologically treated domestic wastewater, the joined effect of various inorganic and organic components practically completely inhibited the elimination of both test substances. Our results suggest that despite their excellent adsorption and photocatalytic properties, our knowledge of the stability of BiOI:BiOCl photocatalyst and the effect of each matrix component and matrices are incomplete and require further investigation.

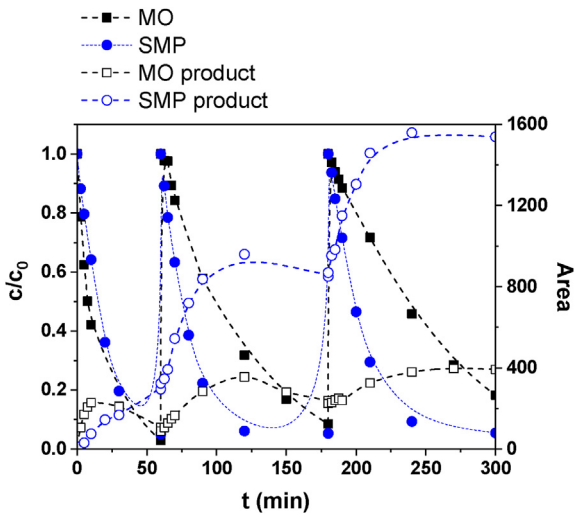


**Fig. 6.** Transformation of MO and SMP and the formation of their product during three cycles.

### 3.9. Toxicity assay

Toxicity studies were performed to check the environmentally friendly use of the prepared photocatalyst. The toxicity of the composite photocatalyst and the treated MO and SMP solution was determined using the *Vibrio fischeri* test organism; the inhibition of the emitted luminescent light intensity is proportional to the degree of toxicity.

The toxicity of 80:20 BiOI:BiOCl photocatalyst was determined during 90 min irradiation without organic substances. After removing the catalyst particles, there was no significant effect of the filtered solutions on the test organism. The inhibition effect was less than 10% and proved that no harmful substances are leached from the catalyst particles (Fig. 8).

The toxicity of $1.0 \times 10^{-4}$ M MO and SMP solutions was negligible. Although the photocatalyst does not pose a risk to the environment, the conversion of both organic substances significantly increased the degree of inhibition effect (Fig. 8), most probably due to the formation of highly toxic intermediates. Our results underline that the toxicity of the formed products during the transformation of each model compound should be given priority. However, for other target compounds, the use of the photocatalyst tested here may be appropriate to remove them without increasing toxicity. All this requires further investigations using various target substances.

### 3.10. Comparison of the efficiency of BiOI:BiOCl and Aeroxide® P25 $TiO_2$

Aeroxide® P25 $TiO_2$ is often used as a "reference" in the case of heterogeneous photocatalysis. The prepared composite photocatalyst efficiency was compared to this widely used, commercially available, well-known material. The photocatalysts (1.5 g $dm^{-3}$) and MO ($1.0 \times 10^{-4}$ M) concentrations were the same in both cases. The relative amount of adsorbed MO was not significant for $TiO_2$ (6%) comparing to that measured for 80:20 BiOI:BiOCl

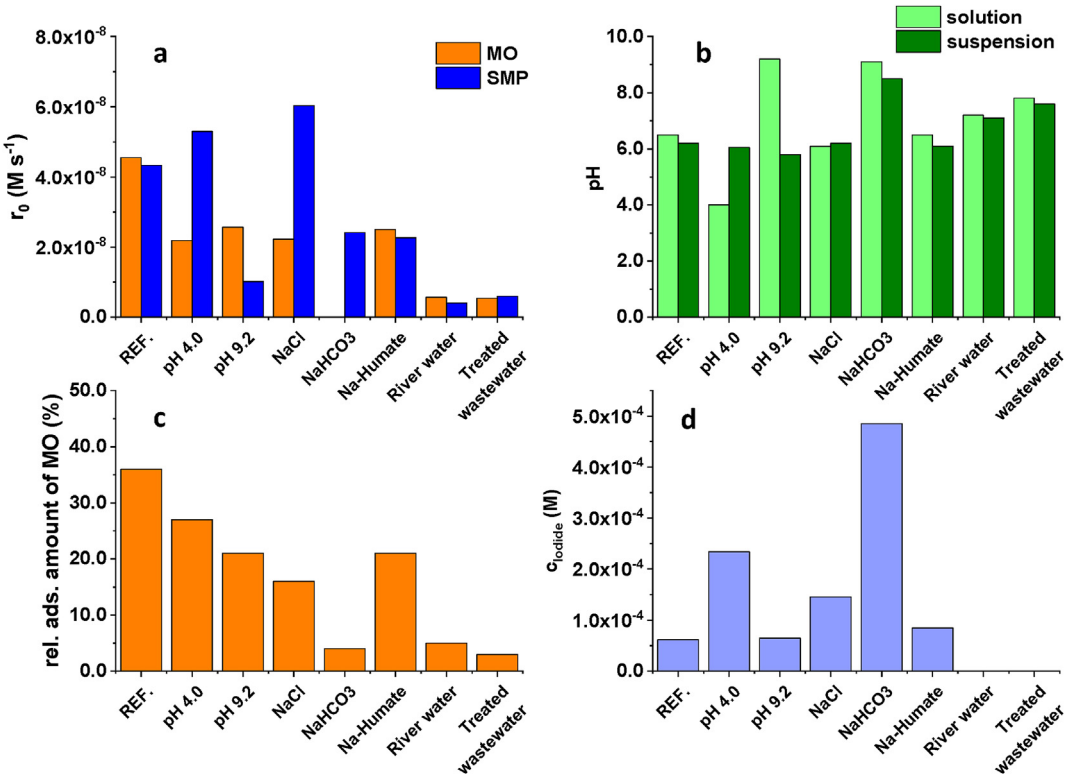


**Fig. 7.** The effect of various matrix components and matrices. a: initial transformation rates; b: pH before and after addition the 80:20 BiOI:BiOCl photocatalyst; c: I concentration after 30 min stirring in dark (determined by spectrophotometry); d: relative amount of adsorbed MO (in the case of real matrices could not be determined due to matrix absorption).

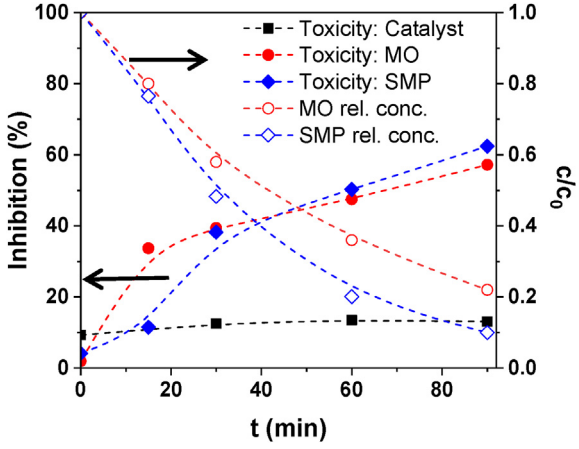


**Fig. 8.** The change of MO and SMP relative concentration ($1.0 \times 10^{-4}$ M) and the degree of the inhibition, using 80:20 BiOI:BiOCl photocatalyst (0.5 g $dm^{-3}$) suspension.

photocatalyst (75%).

Different light sources were applied for the excitation; mercury vapor lamp emitting in the range of 300–400 nm, $5.13(\pm0.34) \times 10^{-7}$ $mol_{photon}$ $s^{-1}$ for the $TiO_2$ and 398 nm UV LED, $5.81(\pm0.03) \times 10^{-6}$ $mol_{photon}$ $s^{-1}$ for the composite photocatalyst). The electric energy required to degrade the concentration by one order of magnitude in a unit volume (100 $cm^3$) was calculated and used for comparison. This value depends not only on the catalyst activity but also on the parameters of the light source. For the calculation, the volume of the treated suspension, the electrical parameters of the light sources, and the time required for the 90% decomposition were used. Using 0.5 g $dm^{-3}$ 80:20 BiOI:BiOCl photocatalyst, this value was 30, and 40 kJ for UV LED and for visible light LEDs, respectively. Similar values (24 and 32 kJ) was determined for SMP. At 1.5 g $dm^{-3}$ concentration of photocatalyst, 30 and 24 kJ decreased to ~12 kJ, about half of the energy requirement calculated for $TiO_2$ (23 kJ), using 15 W mercury-vapor lamp and the same concentration of photocatalyst.

## 4. Conclusions

This study aims to investigate the absorption capacity and activity of BiOCl, BiOI, and BiOI:BiOCl composites for elimination two organic substances MO and SPM. Three light sources were used and compared to decompose MO and SMP as a model compounds: 398 nm UV, cool and warm white visible light LEDs. BiOI and BiOI:BiOCl composites were effective photocatalysts under near-UV and visible light; the best results were obtained using the 80:20 BiOI: BiOCl composite, which showed a similar adsorption capacity as BiOI, but the initial transformation rate of MO was about three times higher than for pure BiOI. There was a significant difference between the light sources' photon flux and the average energy of the emitted photons of the applied LEDs. Thus the comparison was based on the $\Phi_{app}$ values of transformation. In the case of the BiOI and BiOI:BiOCl composite, the obtained $\Phi_{app}$ values were similar for the UV, cool white, and warm white LEDs. All this suggests that BiOI:BiOCl composite can utilize visible and ultraviolet light with similar efficiency.

The reusability was studied during three consecutive cycles, in Milli-Q water. The transformation rate decreased after the first one, but there was no difference between the transformation rates determined in the second and third cycles. The decreased efficiency probably relates to the accumulation of intermediates on the

surface. However, the catalyst does not pose a risk to the environment; the conversion of MO and SMP results in toxic intermediates. Prolonged treatment time is likely to result in the degradation of intermediates and reduction of toxicity.

According to the transformation of 1,4-BQ, the effect of radical scavengers, and formed intermediates, the main transformation way could be the direct charge transfer in both cases, which results in demethylation of MO and $SO_2$ extrusion from SMP. An interesting spectral feature was observed for pure BiOCl; its light absorption extends in the visible region due to the UV light induced formation of oxygen vacancies. This can be the reason of that, under 398 nm irradiation BiOCl showed high activity for the transformation of 1,4-BQ and for SMP opposite that its band gap value is 3.41 eV. It was not observed under visible light radiation.

Using 1.5 g $dm^{-3}$ concentration of the 80:20 BiOI:BiOCl photocatalyst and UV LED emitting at 398 nm, the energy requirement of conversion was significantly lower than for the widely used $TiO_2$ photocatalyst under 300–400 nm UV irradiation, using a mercury-vapor lamp. All this proves that combining these composite catalysts with LED technology can be an energy-efficient solution for removing the well-adsorbed dyes from water. However, the negative effect of the matrix component, especially $HCO_3^-$, raises some questions for practical applicability. Based on these, in the case of wastewaters, pre-treatment can be an essential factor for the efficient application of the investigated photocatalysts.

## Author contributions

Tünde Alapi, Conceptualization, Writing- Reviewing and Editing. Máté Náfrádi, Experimental work, Data evaluation, Writing. Klára Hernádi, Conceptualization. Zoltán Kónya, Providing XRD, DRS and XPS measurements

## Funding

This work was supported by the János Bolyai Research Scholarship of the Hungarian Academy of Sciences, and the new national excellence program of the Ministry for Innovation and Technology (ÚNKP-20-3-SZTE 548, and ÚNKP-20-5-SZTE 639). The research work was sponsored by the National Research, Development and Innovation Office (NKFIH), project number NKFIH OTKA FK 132742.

## Declaration of competing interest

The authors declare that they have no known competing financial interests or personal relationships that could have appeared to influence the work reported in this paper.

## Appendix A. Supplementary data

Supplementary data to this article can be found online at https://doi.org/10.1016/j.chemosphere.2021.130636.

## References

Ahern, J.C., Fairchild, R., Thomas, J.S., Carr, J., Patterson, H.H., 2015. Characterization of BiOX compounds as photocatalysts for the degradation of pharmaceuticals in water. Appl. Catal. B Environ. 179, 229–238. https://doi.org/10.1016/j.apcatb.2015.04.025.

Ahmed, S.N., Haider, W., 2018. Heterogeneous photocatalysis and its potential applications in water and wastewater treatment: a review. Nanotechnology 29. https://doi.org/10.1088/1361-6528/aac6ea.

Akpan, U.G., Hameed, B.H., 2009. Parameters affecting the photocatalytic degradation of dyes using TiO2-based photocatalysts: a review. J. Hazard Mater. https://doi.org/10.1016/j.jhazmat.2009.05.039.

Bárdos, E., Király, A.K., Pap, Z., Baia, L., Garg, S., Hernádi, K., 2019. The effect of the synthesis temperature and duration on the morphology and photocatalytic activity of BiOX (X = Cl, Br, I) materials. Appl. Surf. Sci. 479, 745–756. https://doi.org/10.1016/j.apsusc.2019.02.136.

Chen, J., Loeb, S., Kim, J.H., 2017. LED revolution: fundamentals and prospects for UV disinfection applications. Environ. Sci. Water Res. Technol. 3, 188–202. https://doi.org/10.1039/c6ew00241b.

Cheng, H., Huang, B., Dai, Y., 2014. Engineering BiOX (X = Cl, Br, I) nanostructures for highly efficient photocatalytic applications. Nanoscale 6, 2009–2026. https://doi.org/10.1039/c3nr05529a.

Cornet, J.F., Marty, A., Gros, J.B., 1997. Revised technique for the determination of mean incident light fluxes on photobioreactors. Biotechnol. Prog. 13, 408–415. https://doi.org/10.1021/bp970045c.

Dai, G., Yu, J., Liu, G., 2011. Synthesis and enhanced visible-light photoelectrocatalytic activity of p - N junction BiOI/TiO2 nanotube arrays. J. Phys. Chem. C 115, 7339–7346. https://doi.org/10.1021/jp200788n.

Dai, K., Chen, H., Peng, T., Ke, D., Yi, H., 2007. Photocatalytic degradation of methyl orange in aqueous suspension of mesoporous titania nanoparticles. Chemosphere 69, 1361–1367. https://doi.org/10.1016/j.chemosphere.2007.05.021.

Di, J., Xia, J., Ji, M., Xu, L., Yin, S., Zhang, Q., Chen, Z., Li, H., 2016. Carbon quantum dots in situ coupling to bismuth oxyiodide via reactable ionic liquid with enhanced photocatalytic molecular oxygen activation performance. Carbon N. Y. 98, 613–623. https://doi.org/10.1016/j.carbon.2015.11.015.

Dong, F., Sun, Y., Fu, M., Wu, Z., Lee, S.C., 2012. Room temperature synthesis and highly enhanced visible light photocatalytic activity of porous BiOI/BiOCl composites nanoplates microflowers. J. Hazard Mater. 219–220, 26–34. https://doi.org/10.1016/j.jhazmat.2012.03.015.

Flak, D., Braun, A., Mun, B.S., Park, J.B., Parlinska-Wojtan, M., Graule, T., Rekas, M., 2013. Spectroscopic assessment of the role of hydrogen in surface defects, in the electronic structure and transport properties of TiO2, ZnO and SnO2 nanoparticles. Phys. Chem. Chem. Phys. 15, 1417–1430. https://doi.org/10.1039/c2cp42601c.

Fónagy, O., Szabó-Bárdos, E., Horváth, O., 2021. 1,4-Benzoquinone and 1,4-hydroquinone based determination of electron and superoxide radical formed in heterogeneous photocatalytic systems. J. Photochem. Photobiol. Chem. 407 https://doi.org/10.1016/j.jphotochem.2020.113057.

Ganose, A.M., Cuff, M., Butler, K.T., Walsh, A., Scanlon, D.O., 2016. Interplay of orbital and relativistic effects in bismuth oxyhalides: BiOF, BiOCl, BiOBr, and BiOI. Chem. Mater. 28, 1980–1984. https://doi.org/10.1021/acs.chemmater.6b00349.

Garg, S., Yadav, M., Chandra, A., Sapra, S., Gahlawat, S., Ingole, P.P., Pap, Z., Hernadi, K., 2018a. Biofabricated BiOI with enhanced photocatalytic activity under visible light irradiation. RSC Adv. 8, 29022–29030. https://doi.org/10.1039/c8ra05661g.

Garg, S., Yadav, M., Chandra, A., Sapra, S., Gahlawat, S., Ingole, P.P., Todea, M., Bardos, E., Pap, Z., Hernadi, K., 2018b. Facile green synthesis of BiOBr nanostructures with superior visible-light-driven photocatalytic activity. Materials 11. https://doi.org/10.3390/ma11081273.

Hao, L., Huang, H., Guo, Y., Du, X., Zhang, Y., 2017. Bismuth oxychloride homogeneous phasejunction BiOCl/Bi 12 O 17 Cl 2 with unselectively efficient photocatalytic activity and mechanism insight. Appl. Surf. Sci. 420, 303–312. https://doi.org/10.1016/j.apsusc.2017.05.076.

Hatchard, C.G., Parker, C.A., 1956. A new sensitive chemical actinometer - II. Potassium ferrioxalate as a standard chemical actinometer. Proc. R. Soc. London. Ser. A. Math. Phys. Sci. 235, 518–536. https://doi.org/10.1098/rspa.1956.0102.

Jia, X., Cao, J., Lin, H., Chen, Y., Fu, W., Chen, S., 2015. One-pot synthesis of novel flower-like BiOBr0.9I0.1/BiOI heterojunction with largely enhanced electron-hole separation efficiency and photocatalytic performances. J. Mol. Catal. Chem. 409, 94–101. https://doi.org/10.1016/j.molcata.2015.08.008.

Jiang, Y.R., Lin, H.P., Chung, W.H., Dai, Y.M., Lin, W.Y., Chen, C.C., 2015. Controlled hydrothermal synthesis of BiOxCly/BiOmIn composites exhibiting visible-light photocatalytic degradation of crystal violet. J. Hazard Mater. 283, 787–805. https://doi.org/10.1016/j.jhazmat.2014.10.025.

Jo, W.K., Tayade, R.J., 2014. New generation energy-efficient light source for photocatalysis: LEDs for environmental applications. Ind. Eng. Chem. Res. 53, 2073–2084. https://doi.org/10.1021/ie404176g.

Khaleel, N.D.H., Mahmoud, W.M.M., Hadad, G.M., Abdel-Salam, R.A., Kümmerer, K., 2013. Photolysis of sulfamethoxypyridazine in various aqueous media: aerobic biodegradation and identification of photoproducts by LC-UV-MS/MS. J. Hazard Mater. 244–245, 654–661. https://doi.org/10.1016/j.jhazmat.2012.10.059.

Khan, J.A., Sayed, M., Khan, S., Shah, N.S., Dionysiou, D.D., Boczkaj, G., 2019. Advanced Oxidation Processes for the Treatment of Contaminants of Emerging Concern, Contaminants of Emerging Concern in Water and Wastewater: Advanced Treatment Processes. Elsevier Inc. https://doi.org/10.1016/B978-0-12-813561-7.00009-2.

Konstantinou, I.K., Albanis, T.A., 2003. Photocatalytic transformation of pesticides in aqueous titanium dioxide suspensions using artificial and solar light: intermediates and degradation pathways. Appl. Catal. B Environ. 42, 319–335. https://doi.org/10.1016/S0926-3373(02)00266-7.

Kuhn, H.J., Braslavsky, S.E., Schmidt, R., 2004. International UNION OF pure and applied chemistry - chemical actinometry. IUPAC Tech. Rep. 1–47.

Li, T.B., Chen, G., Zhou, C., Shen, Z.Y., Jin, R.C., Sun, J.X., 2011. New photocatalyst BiOCl/BiOI composites with highly enhanced visible light photocatalytic performances. Dalton Trans. 40, 6751–6758. https://doi.org/10.1039/c1dt10471c.

Liu, C., Wang, X.J., 2016. Room temperature synthesis of Bi4O5I2 and Bi5O7I ultrathin nanosheets with a high visible light photocatalytic performance. Dalton Trans. 45, 7720–7727. https://doi.org/10.1039/c6dt00530f.

Liu, Z., Wang, Q., Tan, X., Wang, Y., Jin, R., Gao, S., 2019. Enhanced photocatalytic performance of TiO2 NTs decorated with chrysanthemum-like BiOI

nanoflowers. Separ. Purif. Technol. 215, 565–572. https://doi.org/10.1016/j.seppur.2019.01.046.
Mezyk, S.P., Neubauer, T.J., Cooper, W.J., Peller, J.R., 2007. Free-radical-induced oxidative and reductive degradation of sulfa drugs in water: absolute kinetics and efficiencies of hydroxyl radical and hydrated electron reactions. J. Phys. Chem. 111, 9019–9024. https://doi.org/10.1021/jp073990k.
Qian, R., Zong, H., Schneider, J., Zhou, G., Zhao, T., Li, Y., Yang, J., Bahnemann, D.W., Pan, J.H., 2019. Charge carrier trapping, recombination and transfer during TiO2 photocatalysis: an overview. Catal. Today 335, 78–90. https://doi.org/10.1016/j.cattod.2018.10.053.
Sergejevs, A., Clarke, C.T., Allsopp, D.W.E., Marugan, J., Jaroenworaluck, A., Singhapong, W., Manpetch, P., Timmers, R., Casado, C., Bowen, C.R., 2017. A calibrated UV-LED based light source for water purification and characterisation of photocatalysis. Photochem. Photobiol. Sci. 16, 1690–1699. https://doi.org/10.1039/c7pp00269f.
Shan, L., Bi, J., Liu, Y., 2018. Roles of BiOCl(001) in face-to-faced BiOI(010)/BiOCl(001) heterojunction. J. Nanoparticle Res. 20 https://doi.org/10.1007/s11051-018-4272-9.
Shen, F., Zhou, L., Shi, J., Xing, M., Zhang, J., 2015. Preparation and characterization of SiO2/BiOX (X = Cl, Br, I) films with high visible-light activity. RSC Adv. 5, 4918–4925. https://doi.org/10.1039/c4ra10227d.
Siao, C.W., Chen, H.L., Chen, L.W., Chang, J.L., Yeh, T.W., Chen, C.C., 2018. Controlled hydrothermal synthesis of bismuth oxychloride/bismuth oxybromide/bismuth oxyiodide composites exhibiting visible-light photocatalytic degradation of 2-hydroxybenzoic acid and crystal violet. J. Colloid Interface Sci. 526, 322–336. https://doi.org/10.1016/j.jcis.2018.04.097.
Singh, S., Sharma, R., Khanuja, M., 2018. A review and recent developments on strategies to improve the photocatalytic elimination of organic dye pollutants by BiOX (X=Cl, Br, I, F) nanostructures. Kor. J. Chem. Eng. https://doi.org/10.1007/s11814-018-0112-y.
Stefan, M.I., 2017. Advanced Oxidation Processes for Water Treatment - Fundamentals and Applications. Water Intelligence. https://doi.org/10.2166/9781780407197. Online.
Tauc, J., 1968. Optical properties and electronic structure of amorphous Ge and Si. Mater. Res. Bull. 3, 37–46. https://doi.org/10.1016/0025-5408(68)90023-8.
Wang, J., Huang, Y., Guo, J., Zhang, J., Wei, X., Ma, F., 2020. Optoelectronic response and interfacial properties of BiOI/BiOX (X=F, Cl, Br) heterostructures based on DFT investigation. J. Solid State Chem. 284 https://doi.org/10.1016/j.jssc.2020.121181.
Wegner, E.E., Adamson, A.W., 1966. Photochemistry of complex ions. III. Absolute quantum yields for the photolysis of some aqueous chromium(III) complexes. Chemical actinometry in the long wavelength visible region. J. Am. Chem. Soc. 88, 394–404. https://doi.org/10.1021/ja00955a003.
Wu, L., Zhang, Q., Li, Z., Liu, X., 2020. Mechanochemical syntheses of a series of bismuth oxyhalide composites to progressively enhance the visible-light responsive activities for the degradation of bisphenol-A. Mater. Sci. Semicond. Process. 105 https://doi.org/10.1016/j.mssp.2019.104733.
Xiao, X., Hao, R., Liang, M., Zuo, X., Nan, J., Li, L., Zhang, W., 2012. One-pot solvothermal synthesis of three-dimensional (3D) BiOI/BiOCl composites with enhanced visible-light photocatalytic activities for the degradation of bisphenol-A. J. Hazard Mater. 233–234, 122–130. https://doi.org/10.1016/j.jhazmat.2012.06.062.
Xiao, X., Liu, C., Zuo, X., Liu, J., Nan, J., 2016. Microwave synthesis of hierarchical BiOCl microspheres as a green adsorbent for the pH-dependent adsorption of methylene blue. J. Nanosci. Nanotechnol. 16, 12517–12525. https://doi.org/10.1166/jnn.2016.12969.
Yang, C., Li, F., Zhang, M., Li, T., Cao, W., 2016. Preparation and first-principles study for electronic structures of BiOI/BiOCl composites with highly improved photocatalytic and adsorption performances. J. Mol. Catal. Chem. 423, 1–11. https://doi.org/10.1016/j.molcata.2016.06.007.
Yang, J., Xie, T., Zhu, Q., Wang, J., Xu, L., Liu, C., 2020. Boosting the photocatalytic activity of BiOX under solar light: via selective crystal facet growth. J. Mater. Chem. C 8, 2579–2588. https://doi.org/10.1039/c9tc05752h.
Yao, S., Wang, J., Zhou, X., Zhou, S., Pu, X., Li, W., 2020. One-pot low-temperature synthesis of BiOX/TiO2 hierarchical composites of adsorption coupled with photocatalysis for quick degradation of colored and colorless organic pollutants. Adv. Powder Technol. 31, 1924–1932. https://doi.org/10.1016/j.apt.2020.02.023.
Yusoff, M.A.M., Imam, S.S., Shah, I., Adnan, R., 2019. Photocatalytic activity of bismuth oxyiodide nanospheres and nanoplates in the degradation of ciprofloxacin under visible light. Mater. Res. Express 6. https://doi.org/10.1088/2053-1591/ab2918.
Zhang, F., Chen, X., Wu, F., Ji, Y., 2016. High adsorption capability and selectivity of ZnO nanoparticles for dye removal. Colloids Surfaces A Physicochem. Eng. Asp. 509, 474–483. https://doi.org/10.1016/j.colsurfa.2016.09.059.
Zhang, Y., Zhang, J., Tang, W., Wang, N., Liu, Y., Guo, H., 2020. Preparation and characterization of hierarchical BiO0.5Cl0.5 with excellent adsorption and photocatalytic abilities for removal of aquatic dyes. Desalin. WATER Treat. 201, 356–368. https://doi.org/10.5004/dwt.2020.25866.
Zhao, Q., Xing, Y., Liu, Z., Ouyang, J., Du, C., 2018. Synthesis and characterization of modified BiOCl and their application in adsorption of low-concentration dyes from aqueous solution. Nanoscale Res. Lett. 13 https://doi.org/10.1186/s11671-018-2480-y.
Zhong, Y., Liu, Y., Wu, S., Zhu, Y., Chen, H., Yu, X., Zhang, Y., 2018. Facile fabrication of BiOI/BiOCl immobilized films with improved visible light photocatalytic performance. Front. Chem. 6, 1–11. https://doi.org/10.3389/fchem.2018.00058.